Int. J. Heat Mass Transfer. Vol. 10, pp. 237–249. Pergamon Press 1967. Printed in Great Britain

VAPOR VOLUME PROFILES IN DEVELOPING TWO-PHASE FLOW

C. C. ST. PIERRE† and S. G. BANKOFF

Argonne National Laboratory, Argonne, Illinois, and Northwestern University, Evanston, Illinois

(*Received* 3 *March* 1966 *and in revised form* 22 *July* 1966)

Abstract—Transverse void fraction distributions and axial, cross-sectional average void fraction data have been obtained for a rectangular flow channel at elevated pressures employing the γ-attenuation technique. The ability of several cross-sectional models and correlations to predict the axial, average void distributions has also been tested. The development of void profiles in both the axial and transverse directions in a flowing two-phase system is of current interest.

NOMENCLATURE

A, cross-sectional area of channel [L^2];
b, channel half width [L];
C, flow parameter, equation (11) [Dimensionless];
C_0, spatial correlation parameter, equation (9) [Dimensionless];
d, pipe diameter, equation (11) [L];
G, volume flow rate defined for equation (8) [L^3/t];
g, gravitational acceleration [L/t^2];
H, total channel length [L];
H_M, mixing cup enthalpy [ML^2/t^2];
K, constant for Bankoff Model modified by Jones [Dimensionless];
K_B, constant for Bankoff Model, equation (4) [Dimensionless];
p, fluid pressure [M/Lt^2];
q, energy flux [M/t^3];
q_e, evaporative component of q_{tot} [M/t^3];
q_h, agitative or heating component of q_{tot} [M/t^3];
q_{sp}, single phase component of q_{tot} [M/t^3];
q_{tot}, total energy flux [M/t^3];
r, constant defined for equation (7) [Dimensionless];
S, velocity ratio (slip) of vapor to liquid, v_g/v_l [Dimensionless];
V_b, bubble rise velocity with respect to the liquid ahead of the bubble, equation (8) [L/t];
V_α, void detector output voltage for void fraction α;
V_E, void detector output voltage for empty channel;
V_F, void detector output voltage for full channel;
v, mass average velocity [L/t];
v_m, mixture velocity [L/t];
v_{vg}, gas drift velocity, equation (13) [L/t];
w, mass flow rate [M/t];
X, quality: ratio of vapor mass flow rate to total mass flow rate [Dimensionless];
Y^*, distance from channel centerline, Y/b [Dimensionless];
z^*, axial distance, Z/H [Dimensionless].

Greek symbols

α, time–average local void fraction [Dimensionless];
γ, density ratio, ρ_g/ρ_l [Dimensionless];
ΔT_d, transition boundary subcooling defined by equation (16) [T];
ΔT_{sub}, inlet subcooling to the test section [T];

† Present address: Department of Chemical Engineering, University of Windsor, Windsor, Ontario.

ΔT_T, transition subcooling, least of ΔT_d, ΔT_{sub} [T];
ϵ, ratio of agitative to evaporative heat fluxes, q_h/q_e [Dimensionless];
η, constant defined in equation (16) [TLt^2/M];
ρ, fluid density [M/L^3].

Subscripts

B, denotes bulk boiling boundary;
g, denotes gaseous or steam phase;
l, denotes liquid or water phase;
0, denotes inlet of test section;
S, denotes thermodynamic saturation conditions;
T, denotes transition boundary.

Superscripts

$*$, denotes dimensionless variable reduced with respect to some characteristic dimension;
$\bar{}$, denotes cross-sectional average of variable.

INTRODUCTION

THIS work was concerned with the acquisition of experimental vapor volume (void) fraction data in a flowing two-phase system. Transverse void fraction distributions and axial, cross-sectional average void fraction data were obtained for a single, rectangular flow channel. A forced-circulation boiling loop was operated at various fixed elevated pressures, inlet flow rates and temperatures. Void profiles were measured employing the γ-attenuation technique.

Several existing models were tested for their ability to predict the axial distribution of cross-sectional average void fraction. Accurate theoretical predictions of steady-state void fraction distributions in both axial and transverse directions are currently of considerable interest in two-phase flow technology.

LITERATURE REVIEW

Innumerable papers have reported data on cross-sectional average void fractions in flowing two-phase systems. However, data on transverse void profiles for developing two-phase flows have been scarce. Axial development of the transverse void profiles has been reported by Christensen under similar conditions [1] and by Morse *et al.* [2], Wright and Zivi [3] and Kagawa and Hada [4] at atmospheric pressure. Kazin [5] obtained radial steam distributions in a vertical tube at elevated pressures. A forced circulation, air–water loop has also been used [6] for obtaining transverse void profiles. A porous bronze tube was used as the test section and air was bubbled into the water continuously along the length of the test section. Recently, Staub and Zuber [7] reported transverse void profiles at elevated pressures employing Refrigerant 22 as the working fluid. In addition, phase and velocity distribution profiles in annular-dispersed flow have been obtained using an isokinetic probe [8].

Methods for predicting quality–void fraction relationships have been both empirical [9] and theoretical [10–13] in nature. Only those correlations and models which were tested for their ability to predict correctly cross-sectional average, steady-state void fractions have been discussed here.

EQUIPMENT

1. *Loop*

The boiling loop (Fig. 1) used in this work was used previously by Christensen [1] and Anderson [14] and consisted essentially of a heated section, steam separator, cross-over, downcomer and return leg constructed mainly of 2-in. diameter schedule-80 stainless steel pipe. The loop could be operated at pressures up to 2000 psia. The heated section comprised a rectangular channel heated electrically with 1000–2000 A a.c. current. A transition piece preceded the test section and provided a smooth flow transition from the 2-in diameter return leg to the rectangular test section.

A 2-in diameter, 24-in long riser followed the

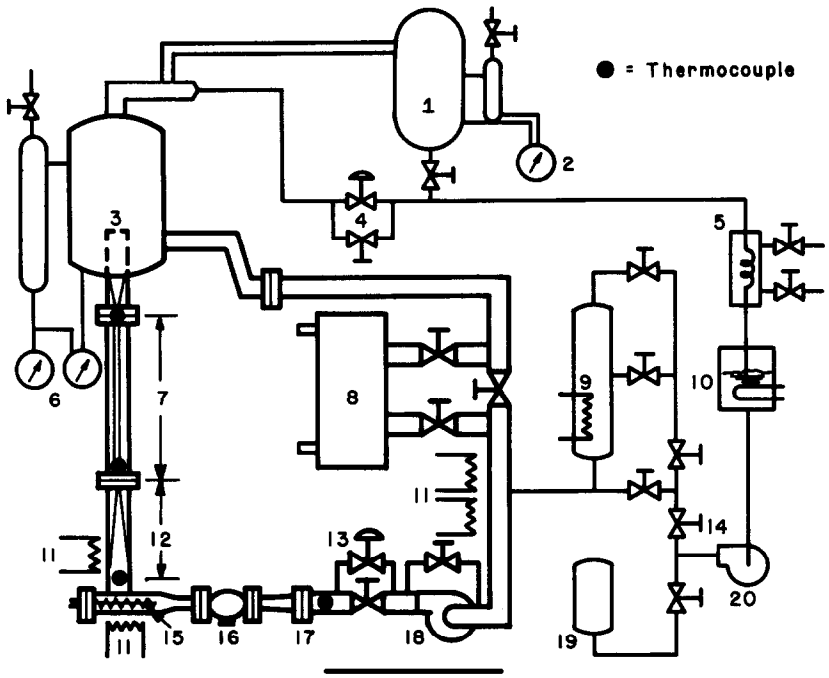

1. Steam surge tank
2. Surge tank level
3. Steam separator
4. Steam bleed valves
5. Water-cooled condenser
6. Pressure and steam separator level
7. Test section
8. Air-cooled heat exchanger
9. Pre-heater and surge tank
10. Water-cooled make-up tank
11. Line heaters
12. Transition length
13. Flow control valve
14. Micrometer valve
15. Calrod heaters
16. Flow meter
17. Orifice flange
18. 100-amp pump
19. Accumulator
20. Make-up pump

FIG. 1. Schematic of loop.

test section and a 4-in diameter, 48-in high steam separator was above the riser. Here the generated steam was bled off and water returned to the recirculation path. The cross-over and downcomer were each approximately 12 ft in length, serving as a recirculation flow path for the water.

In the return leg were located the pump, flow meters, flow control valves and line heaters for inlet temperature control. Forced circulation was provided by a canned rotor pump with a capacity of 50 gpm at 100 psi head. A 2-in air operated main flow valve in parallel with a $\frac{1}{2}$-in manually operated linear valve provided flow control. Inlet temperatures to the test section were controlled by the use of line heaters placed around the loop, the preheater in the surge tank and a heat exchanger on the return leg of the loop. Continuous smooth flow of make-up water to replenish that bled off as steam was provided by a high-pressure feed water pump used in conjunction with an accumulator system. The loop pressure was closely controlled by means of two steam bleed valves in parallel. The bled-off steam was condensed and fed into a water-cooled make-up tank on the suction side of the high pressure feedwater make-up pump. The loop normally took 3–4 h after

start-up to reach operating conditions, while 1–2 h were required for shutdown depending on operating conditions.

The pressure, inlet water temperature, test-section power and water flow rate were the four main parameters which had to be maintained constant for satisfactory operation of the loop. The inlet temperature was the most difficult to control, especially at temperatures near saturation, but the drifts in temperature remained within ± 2 °F. Fluctuations in the loop operating pressure were less than ± 1 psi, the precision watt-meter was frequently checked to maintain constant electrical heating power and the flow was easily controllable at any constant level with fluctuations being less than $\pm$ 0·10 gpm.

The test section assembly (Fig. 2) was constructed from cold-drawn seamless stainless steel tubing, type 304, with the following dimensions: flow area 0·437 × 1·750 in, total axial length 61 in, heated length 49·5 in and the wall thickness only 17 mil. The test section was backed up on all four sides in order to prevent deformation of the thin walls at high pressures.

Two power supplies were employed during this experiment. One supply had a power capability of 93 kW at 60 c/s, with a series output connection giving 33·9 V at 2740 A. The second supply provided 300 kW with an output of 3000 A at 100 V.

2. *Parameter measurement*

The gamma-ray attenuation technique used for measuring void fraction was similar to that employed by Christensen [1]. This method has been described by Hooker and Popper [15] and by Petrick and Swanson [16]. The radiation pellets were standard thulium-170 sources developed at ANL [17]. An excellent discussion of the sources of errors of the gamma-attenuation technique has been given by Christensen [1]. Daily calibrations were made on the electrical components of the void detector system. Errors in gain of the crystal and photomultiplier tube were minimized by maintaining them at a constant ($\pm\frac{1}{2}$ degF) low temperature (40–50 degF). Noise due to thulium source statistics and boiling was eliminated by filtering the output of the current amplifier employing a *m*-derived low-pass filter. Errors due to distributed source spectrum have been estimated to be 1 per cent if the attenuation is computed by a single absorption coefficient. The output of the void detector is nonlinear; hence averaging of the noisy signal can lead to an error. However, for void variations as large as 20 per cent the maximum error is estimated to be less than 1 per cent. There are also errors associated with incompletely known phase distribution and incomplete traversing. If each element of the gamma beam passes through either gas or liquid (approximately true for slug or annular flow), then

$$\alpha = \frac{V_\alpha - V_F}{V_E - V_F}. \tag{1}$$

However, if the phases are homogeneous, as in well-mixed bubble flow, then

$$\alpha = \frac{\ln (V_\alpha / V_F)}{\ln (V_E / V_F)}. \tag{2}$$

Since the void distributions in this study were thought to be closer to the latter case, this equation was used in all void calculations. The error here would have a maximum of 5 per cent at a void fraction of 50 per cent, and is probably much less. This error can be reduced [18, 19] by traversing with a narrow collimating window.

Four liquid temperatures were measured: test section inlet, transition inlet, flow meter inlet and test section exit. All measurements were made with chromel–alumel thermocouples, previously calibrated in a 2000 psia hypsometer, and recorded on a multipoint potentiometric recorder. A student potentiometer was used for accurate measurements and the error in the inlet temperature measurement was believed to be less than ± 1 degF. A turbine flow meter and a 0·5791-in orifice meter were used to measure the inlet flow rate. The saturation

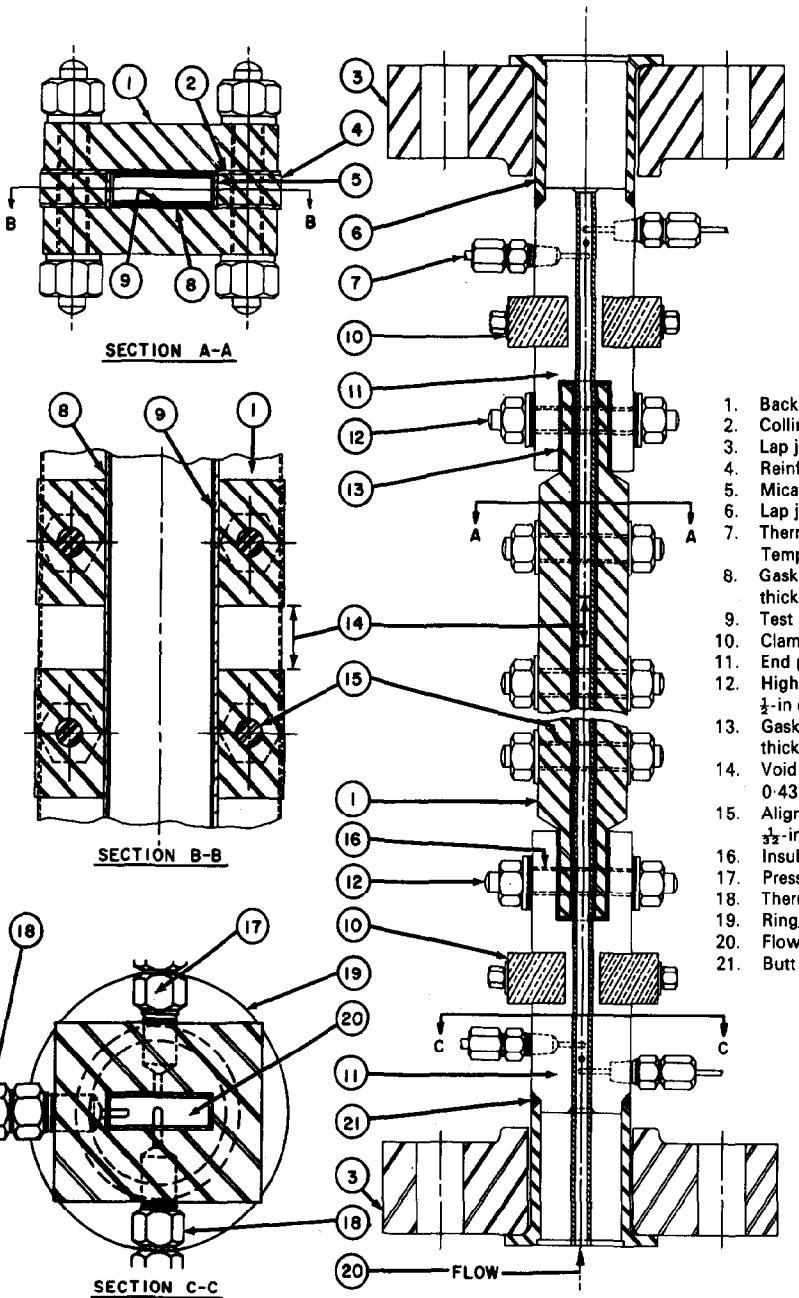

1. Back-up plates; 304 S.S.
2. Collimator strip; 16 gauge, 304 S.S.
3. Lap joint flange; 2 in, 304 S.S.
4. Reinforcing spacer blocks; 304 S.S.
5. Mica-mat insulation; $\frac{1}{8}$-in thickness
6. Lap joint stub end; 2 in, 304 S.S.
7. Thermocouple gland; "Saturation Temperature"
8. Gasket material insulation; $\frac{1}{16}$-in thickness
9. Test section; 17-mil thickness
10. Clamp on bus-bars; copper
11. End piece; 304 S.S.
12. High temperature bolt and nut; steel, $\frac{1}{2}$-in diameter
13. Gasket material insulation; $\frac{1}{16}$-in thickness
14. Void fraction window; 1·125 × 0·437 in
15. Alignment tubing; $\frac{5}{8}$-in diameter, $\frac{1}{32}$-in wall 304 S.S.
16. Insulating cylinder, gasket material
17. Pressure tap, inlet
18. Thermocouple gland; inlet temperature
19. Ring, lap joint flange; 304 S.S.
20. Flow area, 1·750 × 0·437 in
21. Butt weld location

FIG. 2. Test section detail.

Q

pressure in the steam separator was read on a Heise gauge, which was calibrated before, in the middle and at the end of the experimental runs to insure an accuracy of ± 1 psi. A precision watt-meter whose error was estimated to be ± 1 per cent was used to measure average loop power.

VOID FRACTION MEASUREMENT

A narrow ($\frac{1}{32}$ in) void collimating window was used for all steady-state axial and transverse void fraction distributions. Measurements were made at thirteen locations spaced equidistantly along the test channel length and the gamma beam in all cases passed through the 1·750-in depth of the channel. The steady state value of the loop parameters for each run have been summarized in Table 1 and all figures in this paper have been referred to this table.

Table 1. *Summary of steady-state void fraction runs*

Run Number	Pressure p (psia)	Inlet velocity v_0 (ft/s)	Heat flux $\phi \times 10^4$ (Btu/h ft^2)	Inlet subcooling ΔT_{sub} (degF)
1	200	3·78	2·28	0·5
2 and 3	300	2·52	2·28	1·8
4 and 5	400	2·52	4·56	4·8
6	400	2·52	4·56	9·5
7	400	3·78	6·84	1·2
8	400	3·78	6·84	8·1
9	600	3·78	9·12	4·2
10	600	3·78	9·12	12·6
12	800	2·52	4·56	4·9
13	800	3·78	9·12	4·7

Cross-sectional average and transverse void distribution data have been tabulated in reference [20] for all runs.

1. *Cross-sectional average void fractions*

At each axial position the cross-sectional average void fractions were obtained from the transverse measurements by integrating the void distribution across the narrow width of the channel. Due to small misalignments of the test section with respect to the narrow void window, as well as the limited resolution of the γ-attenuation measurement technique, only 80 per cent of the cross-section could be accurately traversed. This would tend to give higher void fractions in the experimental measurements for the downstream portion of the test section, where convex void distributions were present, and lower near the inlet, where concave distributions were found. The magnitude of this error due to incomplete traversing has been discussed previously. Figures 3 and 4 present the axial variation of the cross-sectional average void fractions for all runs. Also, on these graphs are noted the locations of the dimensionless transition boundary, (z^*_T), and bulk-boiling boundaries, (z^*_B), as calculated employing Bowring's analysis [21]. The thermodynamic boiling boundary, (z^*_S), which results from an energy balance and the assumption of thermal equilibrium has also been noted. All theoretical predictions have been indicated by the solid and dashed lines on the figures.

2. *Transverse void fraction distribution*

As mentioned previously, a $\frac{1}{32}$-in collimator window was used in all transverse void measurements across the 0·437-in width of the channel. For this rectangular channel it was assumed that the flow was essentially two-dimensional and the density traverse across the narrow dimension of the channel was equivalent to the phase distribution (i.e. a flat void distribution was assumed to exist across the 1·750-in channel depth).

The axial development of the transverse void fraction distributions has been shown for two typical runs in Figs. 5 and 6. Figure 5 illustrates the development for a case with low inlet subcooling, (1·2 degF) while Fig. 6 is for a run with an appreciable subcooled boiling length ($\Delta T_{sub} = 11{\cdot}1$ degF). The profiles change from concave to convex with increasing axial distance, but the concave profiles persist for a much longer axial distance with increased subcooling (Fig. 6). Since information on transverse void profiles is

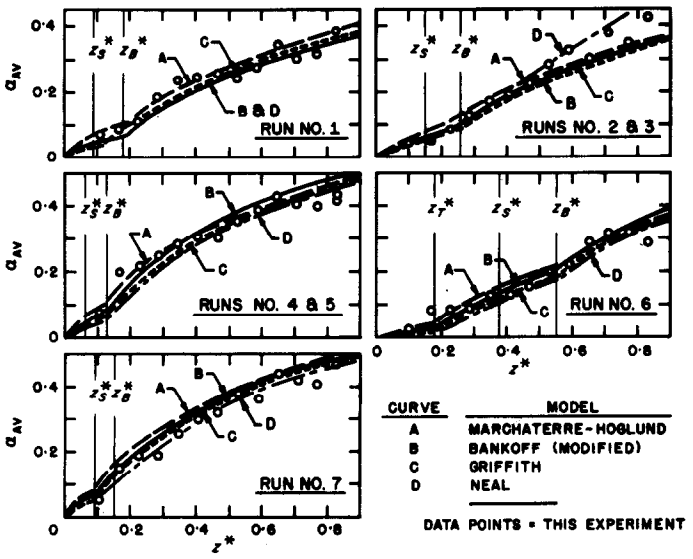

FIG. 3. Steady-state, axial void fraction distributions.

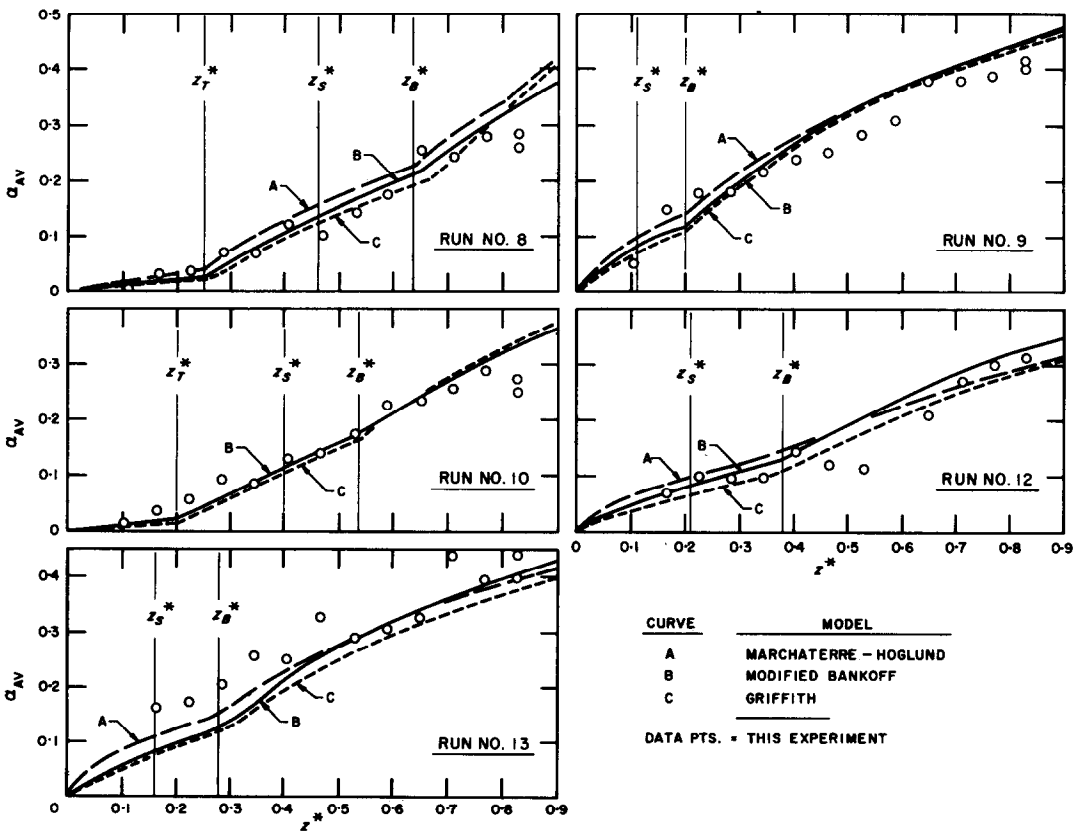

FIG. 4. Steady-state, axial void fraction distributions.

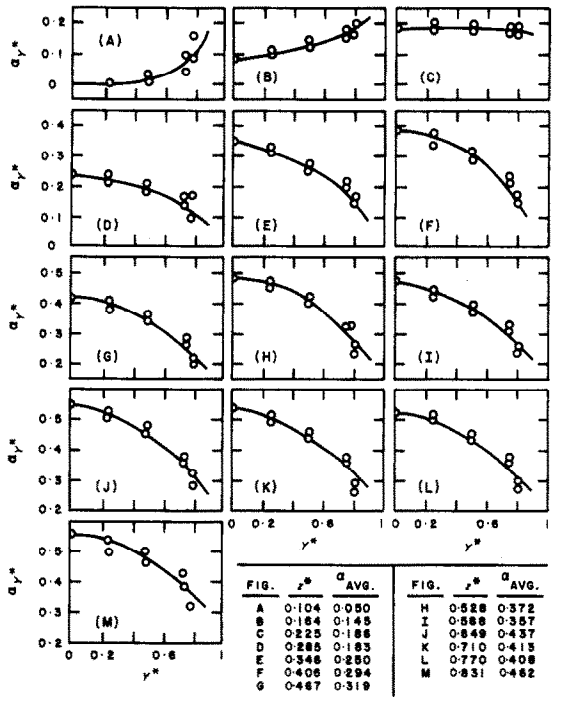

FIG. 5. Transverse void fraction distributions as a function of axial distance for run no. 7.

of considerable interest to workers investigating the prediction of, or effects of local void fraction in two-phase flow systems, the transverse void fraction data for all runs have been tabulated [20].

QUALITY–VOID FRACTION MODELS AND CORRELATIONS

Five different models or correlations were used to calculate the steady-state, cross-sectional average, axial void distributions. A sixth method involved a linear fit of the slip ratio in the subcooled boiling region as a function of enthalpy.

1. *Marchaterre–Hoglund correlation*

This two-phase flow model [9] was based upon an empirical correlation between the Froude number, velocity ratio and volumetric flow rate ratio. Here the average void fraction was given as:

$$\bar{\alpha} = X/[\bar{S}.\gamma + X(1 - \bar{S}\gamma)]. \tag{3}$$

2. *Modified variable density single-fluid model*

Bankoff's variable density model [10], modified by Jones and Dight [22] was a second model tested. Here the mixture is considered to flow as a suspension of bubbles in the liquid, with slip resulting principally from distributional effects. A power-law distribution of both velocity and void fraction was assumed to obtain

$$\bar{\alpha} = \frac{K_B X}{\gamma + (1 - \gamma) X}. \tag{4}$$

Since the slip expression

$$\bar{S} = \frac{1 - \bar{\alpha}}{K_B - \bar{\alpha}} \tag{5}$$

had a discontinuity when $K_B = \bar{\alpha}$, Jones and Dight modified the constant K_B to

$$K = K_B + (1 - K_B)\bar{\alpha}^r \tag{6}$$

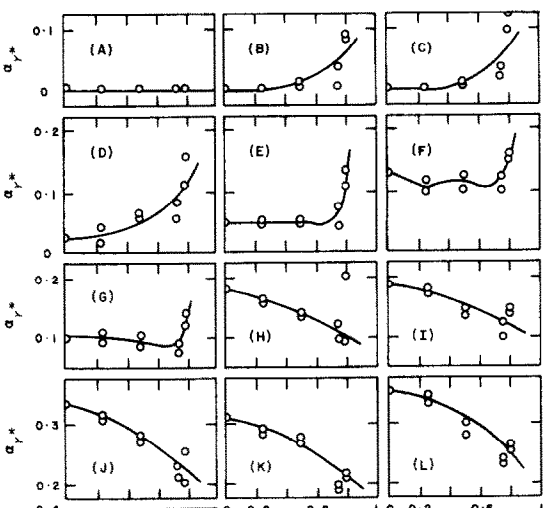

FIG. 6. Transverse void fraction distributions as a function of axial distance for run no. 8.

and the corresponding expression for average void fraction became

$$\bar{\alpha} = \frac{KX}{\gamma + (1-\gamma)X - (1-K)\bar{\alpha}^r}. \quad (7)$$

3. *Griffith model*

Griffith's model [11] for the prediction of low-quality boiling voids was used, since the majority of the runs with low inlet subcooling were probably in the slug flow regime [23]. The validity of employing this model in the high-subcooling runs is doubtful. The average void fraction was given by

$$\bar{\alpha} = G_g/(G_l + G_g + V_b A). \quad (8)$$

4. *Neal model*

Neal's model [12] derived for the bubble and slug flow regimes was based upon the slip ratio resulting from two effects: the difference in gravitational forces acting upon the phases and the existence of radial gradients of void fraction and stream velocity. One of two flow parameters introduced was a spatial correlation factor between α and $\bar{v}_m$

$$C_0 = \frac{\int_0^A \alpha v_m \, dA}{\left[\int_0^A v_m \, dA\right]\left[\int_0^A \alpha \, dA\right](1/A)} = \frac{\overline{\alpha v_m}}{\bar{v}_m \bar{\alpha}} \quad (9)$$

where v_m is the local mixture velocity defined by

$$v_m = \alpha v_g + (1-\alpha) v_l. \quad (10)$$

The second parameter, C, was a measure of the resistance to bubble motion with respect to the liquid, and the bubble rise velocity with respect to $\bar{v}_m$ was given by

$$C\sqrt{[gd(\rho_l - \rho_g)/\rho_l]}. \quad (11)$$

The cross-sectional average gas velocity, $\bar{v}_g$, with respect to laboratory coordinates was then obtained from the two additive components and an expression for slip was derived

$$\bar{S} = \frac{(1-\bar{\alpha})}{(1/C_0 - \bar{\alpha})}\left\{1 + \frac{C}{C_0}\left[\frac{(\rho_l - \rho_g) gd}{\rho_l v_0^2}\right]^{\frac{1}{2}}\right\}. \quad (12)$$

The values of C_0 and C for steam water flows were determined by a least-squares analysis which minimized the error of calculating slip from available data.

5. *Zuber and Findlay model*

Zuber and Findlay [13] performed a similar analysis to that of Neal but extended the consideration of local slip to regimes other than slug flow

$$\frac{G_g}{A\bar{\alpha}} = C_0 \bar{v}_m + \frac{\overline{\alpha v_{vg}}}{\bar{\alpha}} \quad (13)$$

where v_{vg} was defined as the gas "drift velocity" with respect to the volumetric flux density of the mixture, v_m. A plot of G_g/A α vs. v_m was theorized to yield the value of C_0 as the slope and the weighted average drift velocity, $\overline{\alpha v_{vg}}/\bar{\alpha}$, as the intercept, when the local slip does not depend on concentration. In the slug-flow regime, Zuber and Findlay's expression for $\overline{\alpha v_{vg}}/\bar{\alpha}$ was slightly lower than Neal's coefficient. For the bubbly churn-turbulent regime, $\overline{\alpha v_{vg}}/\bar{\alpha}$ was given in terms of the Stokes terminal velocity multiplied by a coefficient which is a function of void fraction. Thus, in order to compare this model with the experimental data, the flow regimes would have to be first determined, and for this reason the average void fractions were not calculated for this model.

6. *Linear variation of slip in the subcooled boiling region*

Since none of the preceding models were developed to cover the case of developing flow in the subcooled region, where the velocity and transverse void profiles are rapidly changing in the axial direction, close agreement between theory and data was not expected. A final model assumed the slip in the subcooled boiling region to be a linear function of the mixing cup enthalpy

to obtain

$$\bar{S} = \bar{S}_T + (\bar{S}_B - \bar{S}_T)(H_M - H_{M,T})/(H_{M,B} - H_{M,T}) \quad (14)$$

where H_M is the mixing cup enthalpy. The enthalpies were calculated according to Bowring's model, while the value of slip at the bulk-boiling boundary was computed using the particular model incorporated in the bulk-boiling region. The value of slip at the transition boundary, S_T was determined by comparison with the corresponding experimental slip ratios calculated for this region.

AXIAL QUALITY DISTRIBUTION CALCULATIONS

1. *Subcooled boiling region*

Bowring's physical model [21] which was based upon experimentally observed detachment of bubbles at low subcooling in heated channels was used in the subcooled boiling region. Two empirical parameters were employed: one determining the ratio of agitative to latent heat flux, and the other relating the subcooling at which bubbles detach to the heat flux and inlet velocity.

The transition boundary, z_T^*, at which subcooled boiling initiates and a rapid rise in void fraction occurs, and the transition subcooling, ΔT_T, at this point were obtained from the lesser of

$$\text{(i) } \Delta T_{sub} \text{ the inlet subcooling, and} \quad (15)$$

$$\text{(ii) } \Delta T_d = \eta q / v_0 \quad (16)$$

which related the subcooling at which bubbles can detach.

Bowring postulated that the total heat flux, q_{tot}, could be divided into an evaporative flux, q_e, on agitative flux, q_h, and a single-phase heat transfer flux, q_{sp}. At the operating conditions of this experiment, q_{sp}, is negligibly small compared to q_e and q_h. Further it was empirically determined that $q_h/q_e = \epsilon \cong 1{\cdot}3$, and this value remained constant throughout the entire subcooled boiling region.

The heating component, q_h, of the total heat flux was used to calculate the axial position, z_B^*, at which the bulk fluid temperature equals the saturation temperature. The evaporative component, q_e, was employed to calculate the axial quality distribution in the subcooled boiling region. Values of quality determined after Bowring's method together with the experimentally determined cross-sectional average void fractions were used to calculate the values of slip in the subcooled boiling region.

2. *Bulk boiling region*

Beyond z_B^*, the bulk boiling boundary, $\epsilon = 0$, $q_e = q_{tot}$ and the axial qualities could be calculated from z_B^* to the test section exit. All qualities calculated for both the subcooled and bulk boiling regions were used in conjunction with the various models tested to calculate the predicted cross-sectional average void distributions in Figs. 3 and 4.

The thermodynamic boiling boundary, z_S^*, was calculated assuming thermodynamic equilibrium, and for this case no subcooled boiling region would exist.

DISCUSSION

There was good agreement between the experimental data and all four models tested in Figs. 3 and 4. In runs (6, 8, 10) an appreciable subcooled boiling length existed. Here the agreement might well be considered fortuitous, on account of the sensitivity of the calculated inception of subcooled boiling to the calculated local axial quality, and also the inapplicability of the bulk-boiling models in this region. However, two significant points may account for this fine agreement between theory and experiment in the subcooled boiling region. Firstly, Bowring in the development of his physical model used extensive subcooled void data obtained on rectangular channels similar in flow area and length to the test section employed in this study. Secondly, the data on these test sections were analyzed, assuming a constant slip throughout the subcooled boiling region, taken to be equal in value to that calcu-

lated at the intersection of the bulk-boiling and subcooled boiling void-fraction curves.

Therefore $(1 + \epsilon)\ S/S_B$, not $(1 + \epsilon)$, was actually used as the correlating parameter in the subcooled boiling region. For this reason, models which predicted correctly the slip value at the bulk boiling boundary gave excellent void fraction predictions in the subcooled boiling region since Bowring's method of correlation decreased the sensitivity of the void fraction predictions in this region on the values of slip.

A discontinuous change in slope is obtained at the bulk boiling boundary for the predicted axial void fraction profiles. This results from the application of Bowring's model to calculate the axial quality distribution. Since Bowring's analysis has the ratio of heating to evaporative heat flux equal to a constant ($\epsilon = 1{\cdot}3$) throughout the subcooled boiling and ϵ equal to zero in the bulk boiling region, a step change in the quality is obtained at the bulk boiling boundary, z_B^*. This suggests that ϵ is not a constant in the subcooled boiling region, but probably is a function of heat flux, temperature or velocity as suggested by Bowring [21].

For the range of qualities, pressures and flow rates covered in this study any one of the four models or correlations could have been used successfully to predict the axial, steady-state, cross-sectional average void distribution. However, at the higher void fractions the Neal model was in closer agreement with the experimental data.

A modification involving an assumption of slip being a linear function of enthalpy in the subcooled boiling region did not markedly improve the theoretical predictions in Figs. 3 and 4, and hence has not been included.

In the axial development of the transverse void fraction distributions the profiles were found to change from concave to convex with increasing axial distance, but the concave profiles persisted for much longer distances with increased subcooling (Fig. 6). This axial development was similar to that found by Christensen [1] under similar conditions and by Morse *et al.* [2], Wright and Zivi [3] and Kagawa and Hada [4] at atmospheric pressure. Staub and Zuber [7] have obtained similar transverse void profiles at elevated pressures employing Refrigerant 22 as the working fluid. Concave transverse void profiles have also been obtained by Kazin [5] where a maximum void concentration was found at a distance from the tube axis of 0·6 of the radius.

Several qualitative observations can be made with regard to the transverse void profiles. The persistence and degree of concavity of the void profiles with axial distance were found to increase with increased inlet temperature subcooling. However, if the transverse void profiles are considered with reference to the bulk average enthalpy, H_m, then the change from concave to convex profiles occurred at a lower H_m for those runs with higher inlet subcooling. This indicated that the presence of entrance effects influenced the formation of transverse void profiles and that the void profile switch from a concave-up to a concave-down shape cannot be related simply to inlet subcooling or bulk average enthalpy. Also, as the shape of the profile passed from concave to convex, points of inflection occurred in the curves. This suggests that for developing flows of this type an expression more complicated than a power law model would be required to describe these profiles near the test section entrance.

However, with increasing axial distance downstream of the point where the convex profile had developed, a power law model could describe the profile. In addition, transverse measurements of axial propagation velocities [24] at a fixed axial position under similar conditions showed that the propagation velocity decreased as the test section wall was approached, and this effect was more pronounced in the downstream regions of the test section. This behavior is consistent with the convex steady-state velocity profiles which are thought to exist in these regions and have been obtained with an isokinetic probe [8] for annular-dispersed flow.

There was parallel behavior in the variation of slip with axial distance and the relative change in void profiles with axial distance. For all concave shaped profiles the slip values were found to be less than or approximately equal to unity. Note that slip values were calculated using the experimentally determined cross-sectional average void fraction and qualities determined after Bowring's method. This suggests that the transverse shape of the void fraction across the test section is an important parameter affecting slip in developing flow.

In Fig. 7 all the void fraction data obtained here are presented as a plot of $G_g/A\,\bar{\alpha} = \bar{v}_g$ vs. $\bar{v}_m$. The circled data points represent for each run the mixture velocity at which a convex void fraction profile was first obtained, and for all downstream points, corresponding to higher mixture velocities the void profiles became more fully developed.

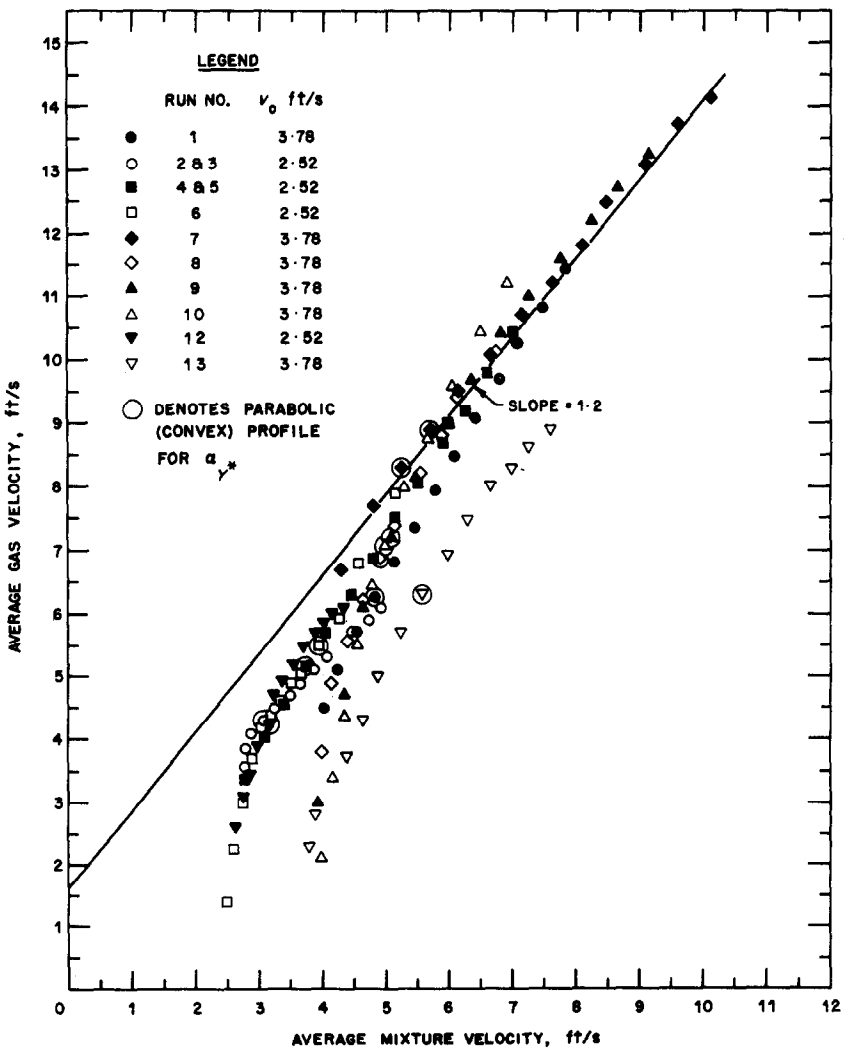

FIG. 7. Cross-sectional average vapor velocity as a function of mixture velocity.

One line with a slope of $C_0 = 1{\cdot}2$ was drawn through the data at the higher $v_{m.\,avg.}$ A second line with $C_0 = 1{\cdot}4$ (not shown) gave slightly better agreement with the data but the calculated liquid velocity profiles are considerably more peaked. It should be noted that the individual curves are all slightly convex. This might result from a decrease in C_0, corresponding to flatter profiles and/or a decrease in local drift velocity, at higher mixture velocities. Both trends might be expected as the mixture velocity increases, in view of the increased wall shear stress.

REFERENCES

1. H. CHRISTENSEN, ANL-6385, Argonne National Laboratory, Argonne, Illinois (1961).
2. A. L. MORSE, R. W. WRIGHT and S. M. ZIVI, RWD-RL-190, Ramo-Wooldridge Research Laboratory, Canoga Park, California (1960).
3. R. W. WRIGHT and S. M. ZIVI, 8977-6031-RU-000, Space Technology Laboratories Inc., Redondo Beach, California (1963).
4. T. KAGAWA, M. HANEDA, H. ANZAI and J. TOMITA, 714th Mech. Engrs Soc. Mtng, Nagasaki City, Japan, Paper 13, p. 141 (1963).
5. L. V. KAZIN, *Teploenergetika* **11**(1), 40 (1964).
6. A. A. KUDIRKA, ANL-6862, Argonne National Laboratory, Argonne, Illinois (1964).
7. F. W. STAUB and N. ZUBER, Quarterly Report, GEAP-4733, General Electric Co., Schenectady, New York (1964).
8. N. ADORNI, G. PETERLONGO, R. RAVETTA and F. A. TACCONI, Report R-91, Centro Informaxioni Studi Esperienze (CISE), Segrate (Milano) (1964).
9. J. T. MARCHATERRE and B. M. HOGLUND, *Nucleonics* **20**, 8 (1962).
10. S. G. BANKOFF, *J. Heat Transfer* **82**C, 265 (1960).
11. P. GRIFFITH, Paper No. 63-HT-20, *A.S.M.E.–A.I.Ch.E. Heat Transfer Conf.* (1963).
12. L. G. NEAL, Report KR-62, Kjeller Research Establishment, Kjeller, Norway (1963).
13. N. ZUBER and J. A. FINDLAY, GEAP-4592, General Electric Company, Schenectady, N.Y. (1964).
14. T. ANDERSON. Personal communication.
15. H. H. HOOKER and G. F. POPPER, ANL-5766, Argonne National Laboratory, Argonne, Illinois (1958).
16. M. PETRICK and B. S. SWANSON, *Rev. Scient. Instrum.* **29**, 1079 (1958).
17. S. S. SIDHU, F. P. CAMPOS and D. D. ZAUBERIS, Special Tech. Publ., No. 223, Am. Soc. for Testing Materials (1958).
18. M. PETRICK, ANL-5787, Argonne National Laboratory, Argonne, Illinois (1958).
19. B. RICHARDSON, ANL-5949, Argonne National Laboratory, Argonne, Illinois (1958).
20. C. C. ST. PIERRE, Ph.D. Thesis, Chemical Engineering Department, Northwestern University, Evanston, Illinois (1965). Also ANL-7041, Argonne National Laboratory, Argonne Illinois (1965).
21. R. W. BOWRING, HPR 29, Institute for Atomenergi, Halden, Norway (1962).
22. A. B. JONES and D. G. DIGHT, KAPL-2208, General Electric Co., New York (1962).
23. P. GRIFFITH, ANL-6796, Argonne National Laboratory, Argonne, Illinois (1963).
24. C. C. ST. PIERRE, M. PETRICK and S. G. BANKOFF, Paper SH-101-104, *Symposium on Two-Phase Flow, Exeter, England* (1965).

Résumé—Les distributions transversales de proportion de vides et la distribution axiale de la proportion moyenne de vides dans une section droite ont été obtenues pour une conduite de section rectangulaire avec des pressions élevées en employant la technique d'absorption de rayons γ. L'aptitude de plusieurs modèles dans la section droite et de plusieurs corrélations pour prédire les distributions axiales de proportion moyenne de vides ont été essayées également. Le développement des profils de vides à la fois dans les directions axiale et transversale à l'intérieur d'un système avec un écoulement diphasique présente un intérêt pratique.

Zusammenfassung—Werte für Querverteilungen des Dampfanteils und Längsverteilungen, gemittelt über den Querschnitt wurden für einen Rechteckkanal und bei erhöhten Drücken mit Hilfe der γ-Attenuationstechnik erhalten. Die Möglichkeit auf Grund verschiedener Querschnittsmodelle und Korrelationen die achsialen, mittleren Dampfverteilungen zu bestimmen, wurde geprüft. Die Ausbildung der Dampfanteilprofile sowohl in achsialer als auch in Querrichtung in einem strömenden Zweiphasensystem ist gegenwärtig von Interesse.

Аннотация—С помощью γ лучей определялись профили концентраций по всем направлениям потока в прямоугольном канале при повышении давления. Также исследовалась достоверность использования некоторых моделей и соотношений для определения распределения концентрации в осевом направлении. Изменение профилей концентраций в осевом и поперечном направлениях представляет большой интерес для задач системы двухфазного потока.